Journal of Hydroscience and Hydraulic Engineering
Vol.12, No .2, November, 1994, 85-100

NUMERICAL SIMULATION OF THE FLOW AROUND THE SPUR DIKES WITH CERTAIN CONFIGURATION AND ANGLES WITH BANK

By

Jian Liu, Akihiro Tominaga and Masashi Nagao

Department of Civil Engineering, Nagoya Institute of Technology
Gokiso-cho, Showa-ku, Nagoya 466, Japan

SYNOPSIS

The flow around the L-head spur dike and spur dikes which have certain angles with the downstream bank is described, using the depth-averaged k-ε model. Extension of computational region and two different categories of local grid elements are employed for treatment of irregular boundaries with staggered grid technique instead of using boundary-fitted transformation. The velocity profiles, streamlines, distribution of turbulent energy and Reynolds stress -uv are obtained, and the calculated results are in good agreement with experimental values. From the point of view of deflecting the stream current away from the bank, the upstream-oriented spur dike is more effective than the others.

INTRODUCTION

The stream erosion is one of the main factors causing flooding inundation. In ordinary circumstances, spur dikes are generally used for protecting river bank from damage. Therefore, the flow around the spur dikes has been studied by means of experiment and numerical simulation. Because of its complexity, numerical studies of the flow around the spur dikes are mostly within confines of the problem of the spur dikes perpendicular to the river bank, however, in actual engineering, the angles between spur dikes and river bank are not always 90°. Generally, the degree of bank protection provided by spur dikes is determined by their length, configuration, orientation angles and spacing between them. It was only evaluated by means of numerical simulation in the present paper that variations of orientation, length and configuration of single spur dike having influence on the flow of the river. Consequently, in order to fully find out the flow characteristics, the flow around the downstream-oriented, normal and upstream-oriented spur dikes (forming 45°, 90°, 135° with downstream bank, separately) is discussed in the present paper, based on basic equations of fluid motion. The flow around the L-head spur dike which extends outward from the bank into the channel and its outer tip turns downstream is also calculated to clarify the influence to the flow due to the configuration's difference. The depth-averaged k-ε model proposed by Rodi (7) is used to close the depth-averaged momentum equations.

The boundary-fitted transformation that transfers an irregular physical domain into a regular computational domain may be used to create a Cartesian grid. However, in accordance with the ideas of Tsakiris et al. (10), the transformation can be tedious, and very difficult to get a proper transformation in certain cases. Moreover, after adopting the transformation, some additional terms have been put into the transformed governing equations, hence, the amount of calculated work will be increased greatly. In order to overcomethe above-mentioned shortcoming, the modified grid system in the present paper is alternatively applied to treat irregular boundaries. The experiments are made for comparison with the calculated values.

MATHEMATICAL MODEL AND DISCRETIZATION

Governing equations

The governing equations for the flow around the L-head spur dike and spur dike which has certain angle with the downstream bank are the Reynolds equations. The steady, depth-averaged forms of the mean-flow equations may be obtained by integrating three dimensional Reynolds equations, over the local water depth. For closing the governing equations, it is necessary to introduce the turbulent representation. When k-ε turbulent model is employed, eddy viscosity ν_t is shown as the function of the depth-averaged turbulent kinetic energy k and its dissipation rate ε (see Rodi (7)). The non-dimensional form of the depth-averaged equations can be written as the following general form in Cartesian coordinates, and summarized in Table 1:

$$\frac{\partial}{\partial x}(u\phi)+\frac{\partial}{\partial y}(v\phi)=\frac{\partial}{\partial x}\left(\Gamma_\phi\frac{\partial\phi}{\partial x}\right)+\frac{\partial}{\partial y}\left(\Gamma_\phi\frac{\partial\phi}{\partial y}\right)+S_\phi \tag{1}$$

where ϕ represents different dependent variables for which the equations are to be solved, Γ_ϕ stands for generalized diffusion coefficients, S_ϕ is source terms.

Table 1 Depth-averaged governing equations

Equation	ϕ	Γ_ϕ	S_ϕ
Continuity	1	0	0
x momentum	u	ν_{eff}	$-F\frac{\partial(z_b+h)}{\partial x}+\frac{\partial}{\partial x}\left(\nu_{eff}\frac{\partial u}{\partial x}\right)+\frac{\partial}{\partial y}\left(\nu_{eff}\frac{\partial v}{\partial x}\right)-\frac{\tau_{bx}}{\rho h}$
y momentum	v	ν_{eff}	$-F\frac{\partial(z_b+h)}{\partial y}+\frac{\partial}{\partial x}\left(\nu_{eff}\frac{\partial u}{\partial y}\right)+\frac{\partial}{\partial y}\left(\nu_{eff}\frac{\partial v}{\partial y}\right)-\frac{\tau_{by}}{\rho h}$
k	k	$1/Re+\nu_t/\sigma_k$	$P_h+P_{kv}-\varepsilon$
ε	ε	$1/Re+\nu_t/\sigma_\varepsilon$	$C_{\varepsilon1}P_h\varepsilon/k+P_{\varepsilon v}-C_{\varepsilon2}\varepsilon^2/k$

$F=gB/Um^2$, $Re=UmB/\nu$, $\nu_t=C_\mu k^2/\varepsilon$, $\nu_{eff}=1/Re+\nu_t$, $\tau_{bx}=\rho C_f u(u^2+v^2)^{1/2}$,

$\tau_{by}=\rho C_f v(u^2+v^2)^{1/2}$, $C_f=n^2g/h^{1/3}$, $C_k=1/C^{1/2}$, $C_\varepsilon=C_{\varepsilon2}C_\mu^{1/2}/(e^*\sigma_t)^{1/2}/C_f^{3/4}$,

$P_{kv}=C_k[C_f(u^2+v^2)]^{3/2}/h$, $P_{\varepsilon v}=C_\varepsilon[C_f(u^2+v^2)]^2/h^2$,

$$P_h=\nu_t\left[2\left(\frac{\partial u}{\partial x}\right)^2+2\left(\frac{\partial v}{\partial y}\right)^2+\left(\frac{\partial u}{\partial y}+\frac{\partial v}{\partial x}\right)^2\right],\ C_\mu=0.09,\ C_{\varepsilon1}=1.44,\ C_{\varepsilon2}=1.92,$$

$\sigma_k=1.0$, $\sigma_\varepsilon=1.3$, $e^*=0.15$, $\sigma_t=0.9$

In Table 1, except fluid density ρ, other variables are separately normalized by the mean bulk velocity Um and width of inlet section B. The Reynolds number for the calculation was based on Um, B and kinematic viscosity ν. h is the local water depth. z_b is the bottom elevation. C_μ, $C_{\varepsilon1}$, $C_{\varepsilon2}$, σ_k, σ_ε, e^*, δ_t, C_k, C_ε are standard coefficients for the model obtained by McGuirk et al. (4). τ_{bx}, τ_{by} are the bed shear stress components in x and y coordinates, respectively. C_f is the friction coefficient, calculated from the Manning law. n is the Manning roughness coefficient (=0.009 in the present paper based on the experiment). g is the gravitational acceleration.

Discretization Procedure

The equations in Table 1 are discretized by utilizing control volume approach and staggered grid system predicted by Patankar et al. (5). It is necessary to mention that, the scalar grid elements neighbor closely to the upstream and downstream sides of the oriented spur dike are right-triangular. The scalar variables (excluding pressure and water depth) lie on the gravity centers of the right-triangular elements, pressure and the water depth are at the middle point of the hypotenuse, u and v are at the middle points of every sides of the elements; thus, u and v control volumes close to the oriented spur dike are trapezoid. Although this staggered grid system complicates the programming and implementation of the solution algorithm, it makes evaluation of the pressure gradients easy in solving the velocity field, and velocities are conveniently located for the calculation of convective fluxes; moreover, facilitates treatment of the irregular boundaries. Fig. 1 shows the staggered grid system with rectangular, trapezoid and right-triangular control volumes for discretizing momentum equations, continuity equation, k and ε equations, separately. For example, the momentum equation of x-direction can be respectively integrated over the rectangular control volume and trapezoid control volume shown in Fig. 1(a), it yields the following local integral conservation equations:

integral result over rectangular control volume,

$$\begin{aligned}
&\Delta y\left(u^2\right)_{i+1/2,j} - \Delta y\left(u^2\right)_{i-1/2,j} + \Delta x(uv)_{i,j+1/2} - \Delta x(uv)_{i,j-1/2} = \\
&\Delta y\left(\Gamma_u \frac{\partial u}{\partial x}\right)_{i+1/2,j} - \Delta y\left(\Gamma_u \frac{\partial u}{\partial x}\right)_{i-1/2,j} + \Delta x\left(\Gamma_u \frac{\partial u}{\partial y}\right)_{i,j+1/2} - \Delta x\left(\Gamma_u \frac{\partial u}{\partial y}\right)_{i,j-1/2} \\
&-F\Delta y\left[\left(z_b + h\right)_{i+1/2,j} - \left(z_b + h\right)_{i-1/2,j}\right] + \Delta y\left(\nu_{eff} \frac{\partial u}{\partial x}\right)_{i+1/2,j} - \Delta y\left(\nu_{eff} \frac{\partial u}{\partial x}\right)_{i-1/2,j} \\
&+\Delta x\left(\nu_{eff} \frac{\partial v}{\partial x}\right)_{i,j+1/2} - \Delta x\left(\nu_{eff} \frac{\partial v}{\partial x}\right)_{i,j-1/2} - \Delta x\Delta y \frac{\tau_{bx}}{\rho h_{i,j}}
\end{aligned} \tag{2}$$

integral result over trapezoid control volume,

$$\begin{aligned}
&\Delta y\left(u^2\right)_{i+1/2,jb} + \Delta x(uv)_{i-1/2,jb+1/2} + \Delta x\left[(uv)_{i+1/2,jb+1/2} - (uv)_{i+1/2,jb-1/2}\right]/2 = \\
&\Delta y\left(\Gamma_u \frac{\partial u}{\partial x}\right)_{i+1/2,jb} - \Delta y\left(\Gamma_u \frac{\partial u}{\partial x}\right)_{i-1/2,jb} + \Delta x\left(\Gamma_u \frac{\partial u}{\partial y}\right)_{i-1/2,jb+1/2} \\
&+\Delta x\left[\left(\Gamma_u \frac{\partial u}{\partial y}\right)_{i+1/2,jb+1/2} - \left(\Gamma_u \frac{\partial u}{\partial y}\right)_{i+1/2,jb-1/2}\right]/2 \\
&-F\Delta y\left[\left(z_b + h\right)_{i+1/2,jb} - \left(z_b + h\right)_{i-1/2,jb}\right] \\
&+\Delta y\left(\nu_{eff} \frac{\partial u}{\partial x}\right)_{i+1/2,jb} - \Delta y\left(\nu_{eff} \frac{\partial u}{\partial x}\right)_{i-1/2,jb} + \Delta x\left(\nu_{eff} \frac{\partial v}{\partial x}\right)_{i-1/2,jb+1/2} \\
&+\Delta x\left[\left(\nu_{eff} \frac{\partial v}{\partial x}\right)_{i+1/2,jb+1/2} - \left(\nu_{eff} \frac{\partial v}{\partial x}\right)_{i+1/2,jb-1/2}\right]/2 - \Delta x\Delta y \frac{\tau_{bx}}{\rho h_{i,jb}}
\end{aligned} \tag{3}$$

Similarly, the discretized form of other governing equations can be derived by integrating over their respective control volumes shown in Fig. 1(b) and Fig. 1(c).

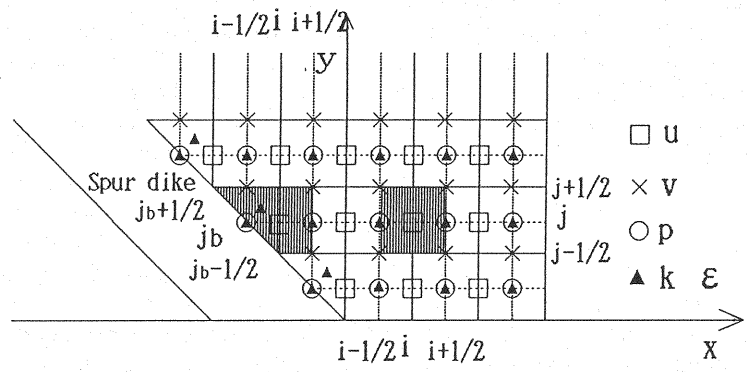

(a) for x momentum equation

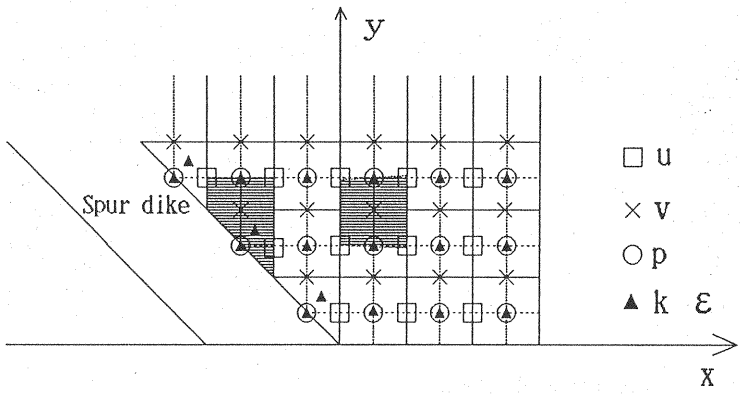

(b) for y momentum equation

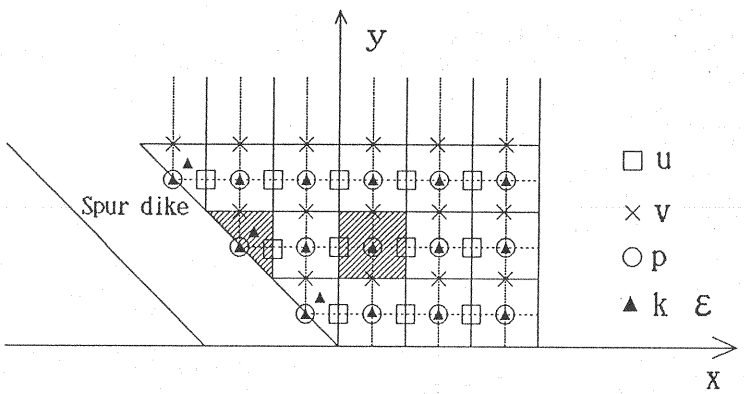

(c) for continuity equation, k and ε equations

Fig. 1 Control volume

CALCULATIONAL IMPLEMENTATION AND BOUNDARY TREATMENT

Calculated procedure

The pressure field is computed by using Van Doormaal and Raithby's SIMPLEC (11) which is a modified version of SIMPLE algorithm proposed by Patankar and Spalding (5). The difference between the two algorithm is that the certain terms produced in inducing the formula of velocity correction by adopting SIMPLE algorithm are made so-called "consistent" treatment, consequently, it is no longer necessary to conduct under-laxation for the pressure correction, resulting in a substantial improvement in rate of convergence based on exposition of Latimer et al. (3). The solution to discretized equations is solved by alternating direction implicit (ADI) scheme. In order to further accelerate the iterative convergence rate, block correction technique (BCT) proposed by Tao (8) is employed. BCT is defined as additional correction method in which the influence of all boundary conditions is delivered to the internal region within one round iteration and it solves a tridiagonal matrix algorithm (TDMA) only once. The mathematical basis of BCT is additional correction method to solve algebraic equation. Its basic idea is that two dimensional problem simplifies quasi-one dimensional problem. But, BCT can not be popularized to solve three dimensional problem. The region located in the spur dike is treated by means of extension of computational region presented by Patanker(6), that is, the diffusion coefficients Γ_ϕ in the region are given one very large number. Thus, it can reflect effectively the influence to the flow by the spur dike, and avoid the decline of the accuracy due to adoption of coordinate transformation for the irregular boundaries as well.

Boundary treatment

The flow around the spur dike belongs to elliptic problem. The boundary conditions of the inlet section, outlet section and solid wall of the calculated region shown in Fig. 2 can be given as follows (with dimensionless):

inlet section:

$$Uin=(1.0+1/7)\times f(y)^{1/7},\ f(y)=y,\ \text{when } y<0.5,\ \text{else } f(y)=1.0-y \tag{4}$$

$$v=0.0 \tag{5}$$

$$k=k_0=1.5\times(0.05\times Uin)^2 \tag{6}$$

$$\varepsilon=\varepsilon_0=C_\mu k_0^{3/2}/0.036 \tag{7}$$

outlet section:

$$\frac{\partial u}{\partial x}=\frac{\partial v}{\partial x}=\frac{\partial k}{\partial x}=\frac{\partial \varepsilon}{\partial x}=0,\ \text{h is specific} \tag{8}$$

solid boundaries:

$$u=v=k=\varepsilon=0 \tag{9}$$

In principle, it is possible to solve the flow around the spur dike according to the above-mentioned boundary conditions. But, under the condition of the high Reynolds number, it is necessary that excessive number of grid nodes in the immediate vicinity of solid wall to reach a higher accuracy.

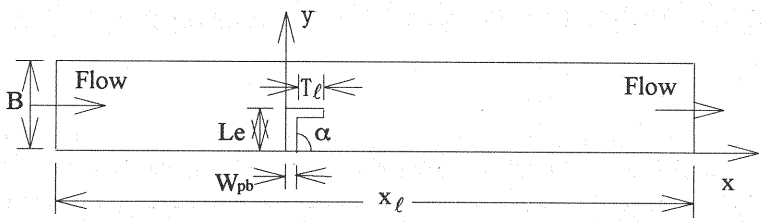

Fig.2 Definition of calculated region

In order to decrease the amount of computational work, the universal logarithmic law is used to treat the calculated regions near to solid wall. It is stated that, in the vicinity of the upstream and downstream faces of the oriented spur dike, the velocity and distance from the faces used for solving the friction velocity $u*$ are V_b and Δn shown in Fig. 3 (see Iwasa et al. (2)). V_b is the component parallel to the face of the oriented spur dike of the vector V located at the center of the triangular control volume, Δn is the distance normal to the face of the spur dike. Details of the treatment of k equation are given in the paper of Chieng et al. (1). The value of ε in the near-wall element was approximated under local equilibrium conditions as:

$$\varepsilon=k_p^{3/2}/C_l y_p \tag{10}$$

where C_l is empirical coefficient ($=C_\mu^{3/4}/\kappa$, κ is von Karman constant), k_p is the value of turbulent kinetic energy at node point P of the element adjacent to the wall. y_p is the distance normal to the wall.

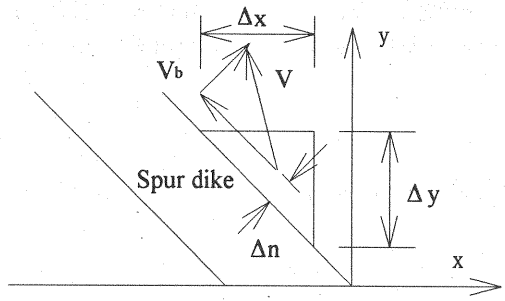

Fig. 3 Calculation of the friction velocity $u*$ near to the oriented spur dike.

EXPERIMENTAL PROCEDURE

The various cases shown in Table 2 are measured and calculated to determine the relative ability of the single spur dikes of varying length, orientation angle and configuration. These conditions are chosen to deflect the main stream current away from the bank and to affect the size of recirculation zones. The experiments were conducted in a tilting flume with 8m length and 0.3m×0.4m cross section. The spur dikes were separately attached to the bottom and one of the side wall of the flume according to the cases in Table 2 (except the normal spur dikes whose non-dimensional length are 0.4 and 0.2, respectively). The measured range was from 1.2m upstream from the upstream side of the spur dike base to 3m downstream from the downstream side of the spur dike base. In the range, the flow was fully developed. The discharge was about 3.6 l/s thus that the water depth of the outlet section was 9cm or so. An electromagnetic velocity meter was used for velocity measurements in the manner as 9 points (interval distance is 3cm) in transverse direction and 2 points of 2cm and 7cm from the bottom in depthwise direction. The measured time at every measured point is 41s. The output signals were

digitized by using an A-D converter with sampling frequency 100Hz. In addition, the water depth was measured by using a digital point gage at the section which y= 3, 9, 15, 21, 27cm in transverse direction.

Table 2 Summary of the experimental and calculated condition

Type / Parameter	Normal spur dike	L-head spur dike	Downstream-oriented spur dike	Upstream-oriented spur dike
Dike size $L_a \times W_{pb}$ (cm×cm)	15×1.8, 12×1.8, 6×1.8	15×1.8, Tip length T_l=3.6	21.2×2.54	21.2×2.54
Relatively effecive length L_e/B (cm)	0.5, 0.4, 0.2	0.5	0.5	0.5
Angle with downstream bank (°)	90, 90, 90	90	45	135
Discharge Q (cm^3/s)	3580, 3580, 3580	3580	3580	3580
Water depth of outlet (cm)	9.0, 9.0, 9.0	9.1	9.1	9.0

In Table 2, normal spur dikes include three different length (without specific comment, normal spur dike refers to the straight spur dike whose non-dimensional length is 0.5 and which forms 90° with the bank). La is the axial length of the spur dike; Le is the effective length defined as the component of total dike length measured perpendicular to the bank from the base to the tip of the spur dike. W_{pb} is the base width parallel to the bank. Tip length of L-head spur dike is the spur dike tip length excluding the main body width which is the distance between the upstream and downstream faces of the spur dikes. The main body width of all spur dikes are 1.8cm. The width of the flume B = 30cm.

COMPUTATION AND DISCUSSION OF RESULTS

The calculated and measured values are non-dimensional ones without specific comment in this section. The depth-averaged velocity and water depth (with dimension) distribution based on calculated results and measured data are depicted in Fig. 4 and Fig. 5, respectively. It is necessary to mention that the experimental values of the velocities are the depthwise average values of 2cm and 7cm from the bottom. It is apparent that the flow behind the spur dike indicates three-dimensional behavior with longitudinal vortices, as shown by Tominaga el al. (9). However, the depth-averaged streamwise velocity could be reasonably obtained by this two points method because of small difference between the values of 2cm and 7cm levels. On the other hand, the depth-averaged lateral velocity might be less accurate than the streamwise one, since the lateral velocity component has relatively small magnitude compared with the difference between the values of the two levels. The calculated values are in good agreement with the experimental data. It can be found that the calculated results of the downstream-oriented spur dike tally better with the measurements. However, for other spur dikes, in the vicinity of their downstream faces, the calculated water depth are slightly larger than the experimented values, and the calculated velocities are slightly smaller than the experimented values. The errors between calculated values and experimental data are about 3-8%. Fig. 6 shows the calculated longitudinal velocity profiles at x/B=0.8 and lateral velocity profiles at y/B=0.75 for various types of spur dikes. We can found that under the same effective length, the changing of velocity caused by the orientation angle is more remarkable than the one caused by the configuration, especially, the variation of the upstream-oriented spur dike is the biggest; on the other hand, with a decrease of the effective length (normal spur dikes only), the minimum and maximum velocities will be swiftly changed. The calculated streamlines are depicted in Fig. 7 (the scale of streamwise and crosswise directions is 1:2.5). The sizes of the recirculation zones of the upstream-oriented spur dikes are larger than those of the other spur dikes under the same effective length. From the point of view of the recirculation length of the

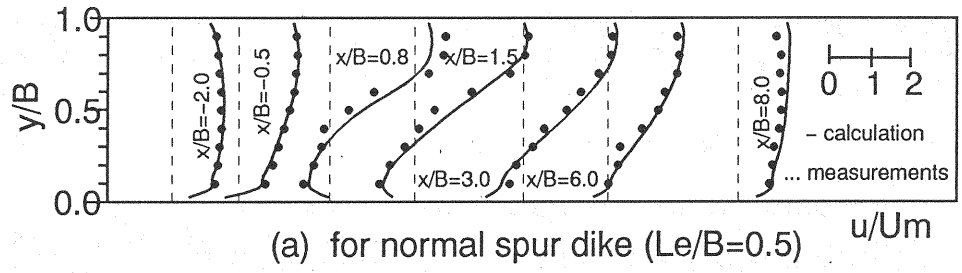

(a) for normal spur dike (Le/B=0.5)

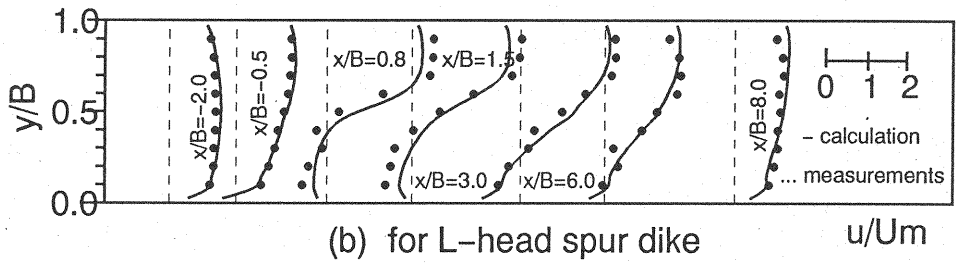

(b) for L-head spur dike

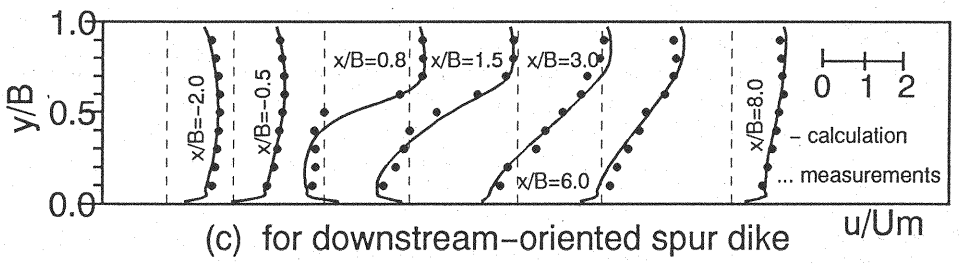

(c) for downstream-oriented spur dike

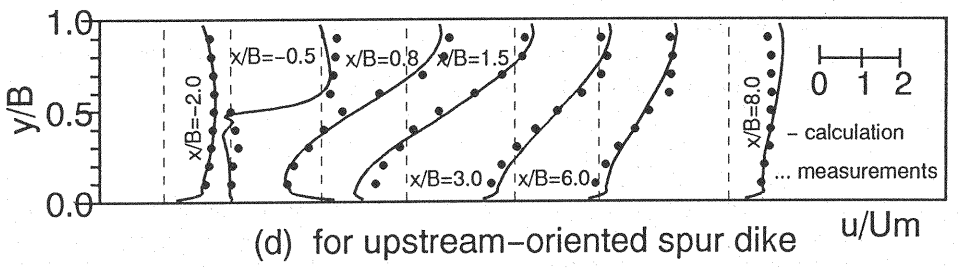

(d) for upstream-oriented spur dike

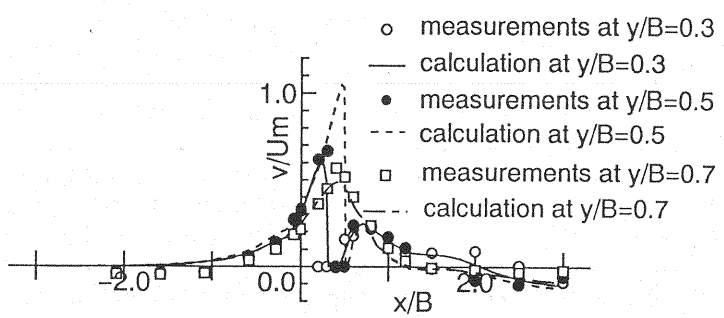

(e) lateral velocity profiles near to downstream-oriented spur dike

Fig. 4 Calculated and measured velocity profiles for the flow around the spur dikes

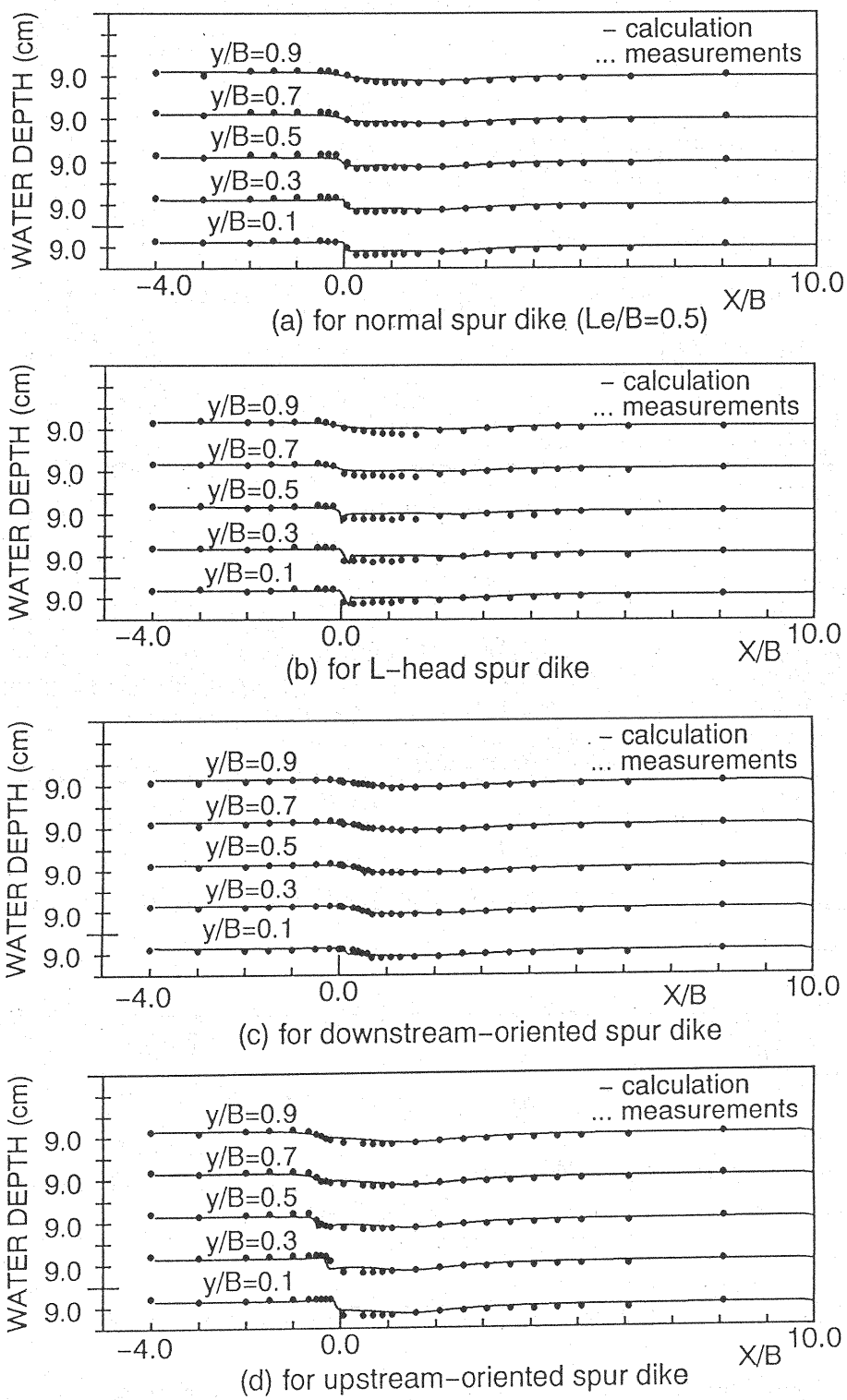

Fig. 5 Calculated and measured longitudinal water level variation

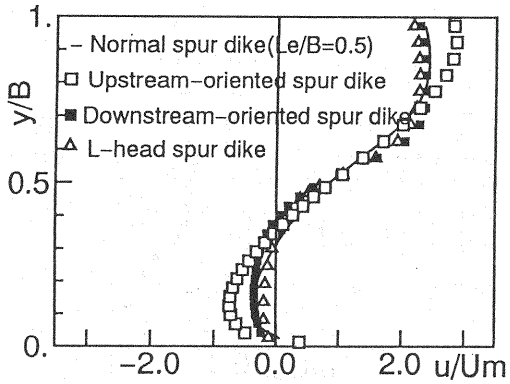

(a) for same effective length

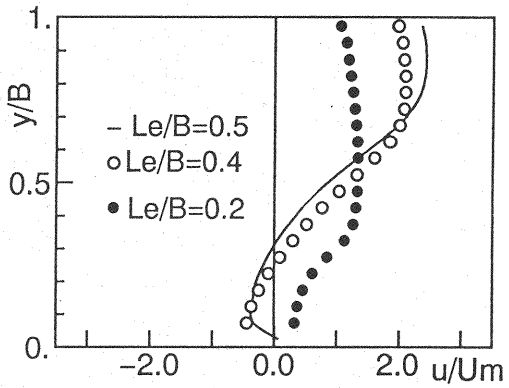

(b) for different effective length for normal spur dikes

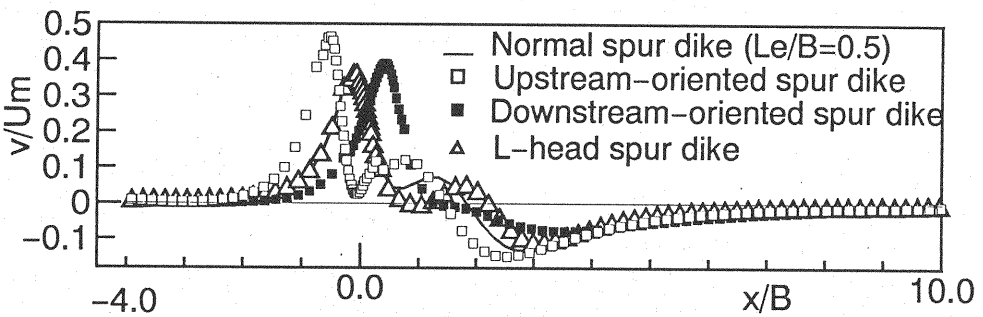

(c) for same effective length

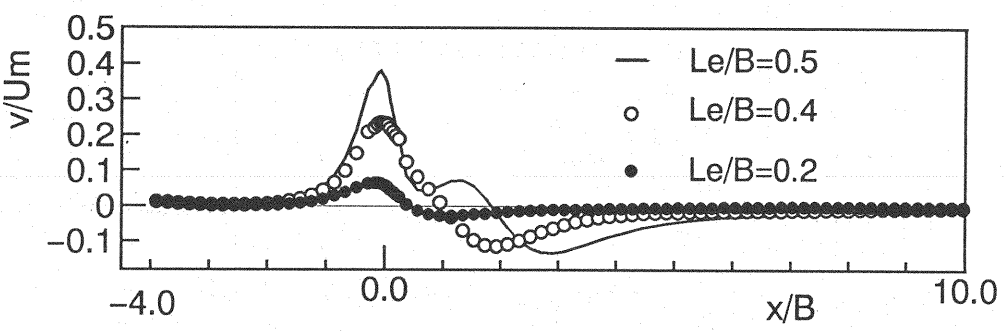

(d) for different effective length for normal spur dikes

Fig. 6 Calculated streamwise velocity profiles at x/B=0.8 and lateral velocity profiles at y/B=0.75 for the flow around the various spur dikes

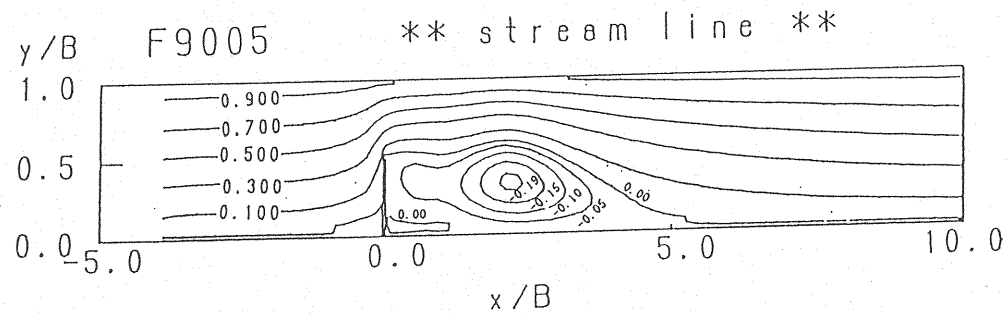

(a) for normal spur dike(Le/B=0.5)

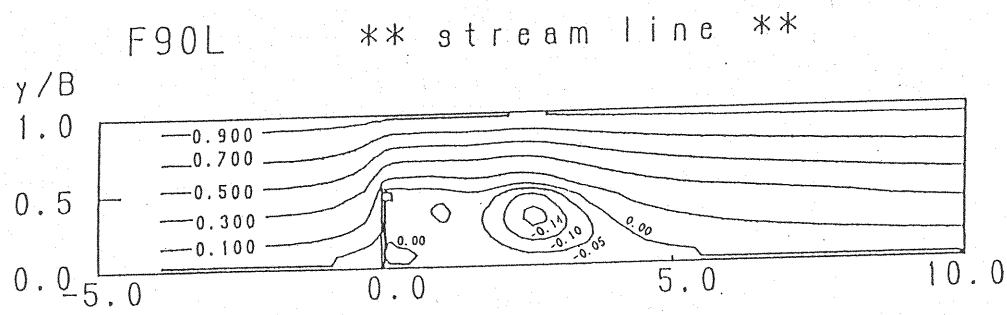

(b) for L-head spur dike

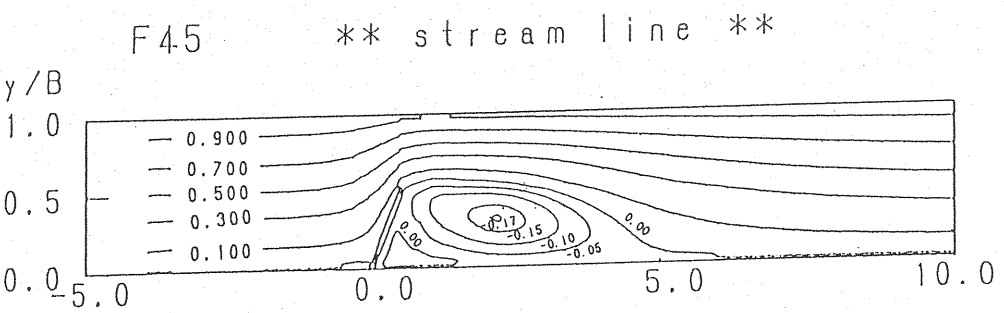

(c) for downstream-oriented spur dike

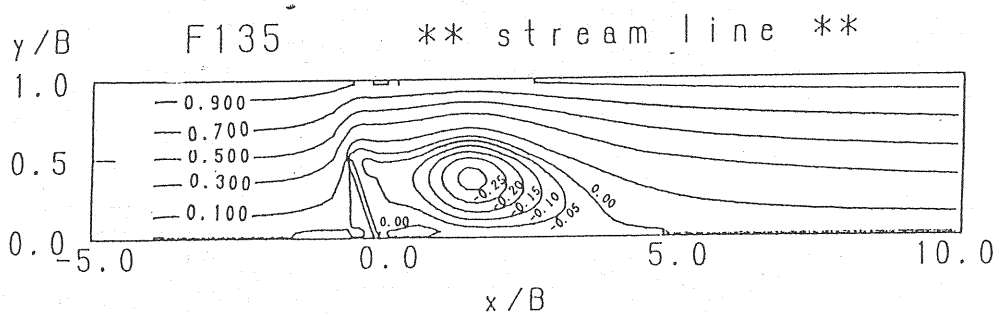

(d) for upstream-oriented spur dike

Fig. 7 Calculated streamlines for the flow around the spur dikes

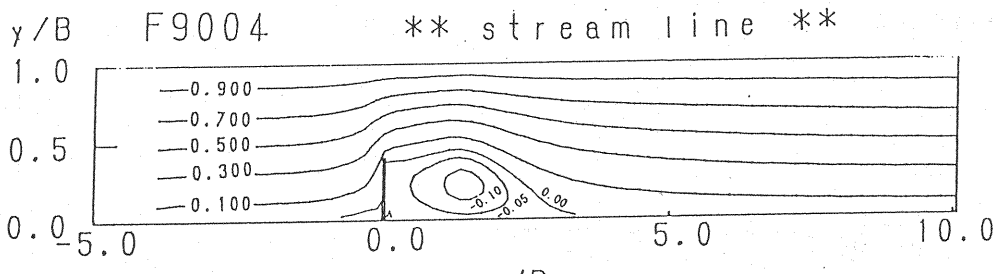

(e) for normal spur dike(Le/B=0.4)

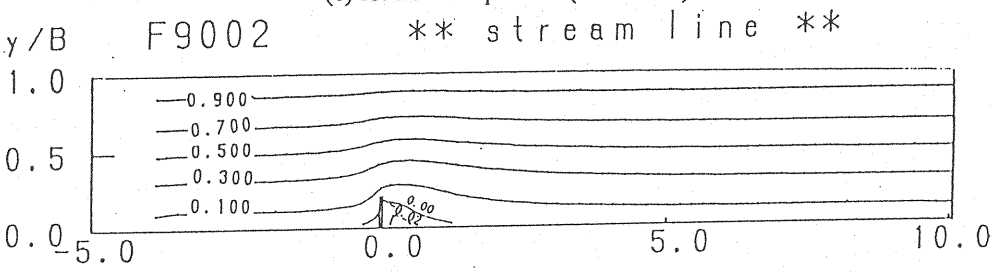

(f) for normal spur dike(Le/B=0.2)

Fig.7 continued

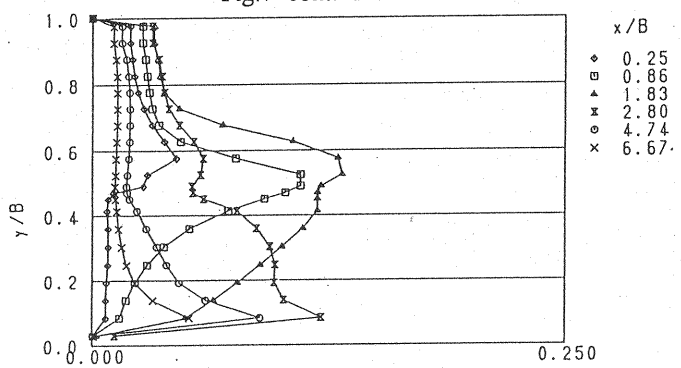

(a) for L-head spur dike

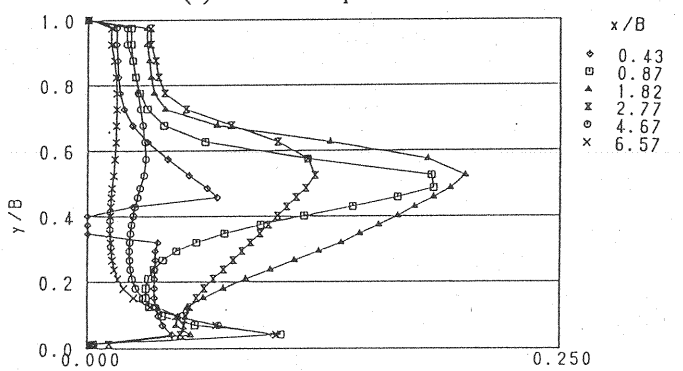

(b) for downstream-oriented spur dike

Fig. 8 Calculated turbulent kinetic energy profiles of L- head spur dike and downstream-oriented spur dike

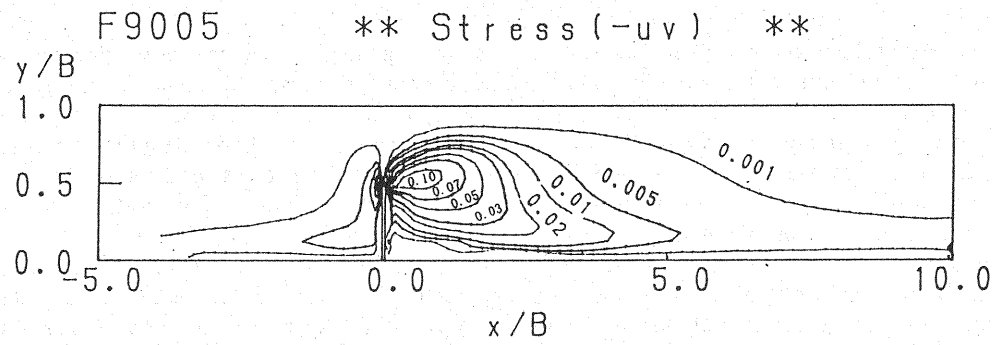

(a) for normal spur dike

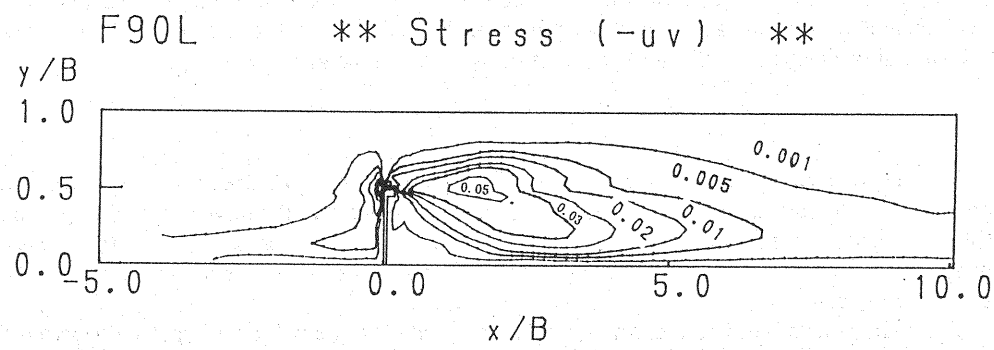

(b) for L-head spur dike

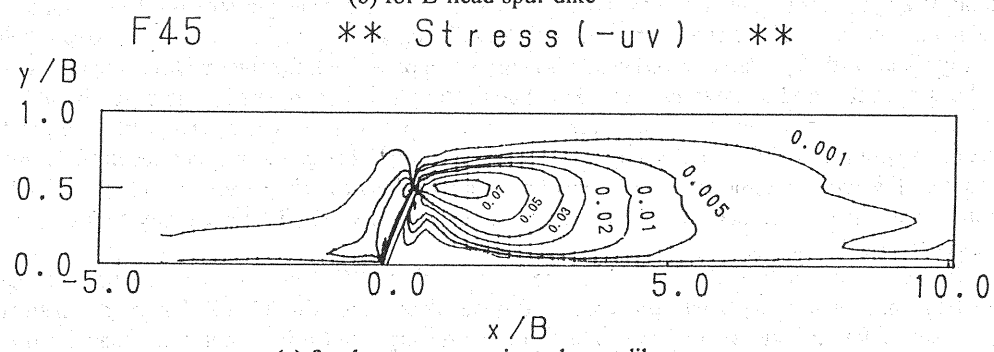

(c) for downstream-oriented spur dike

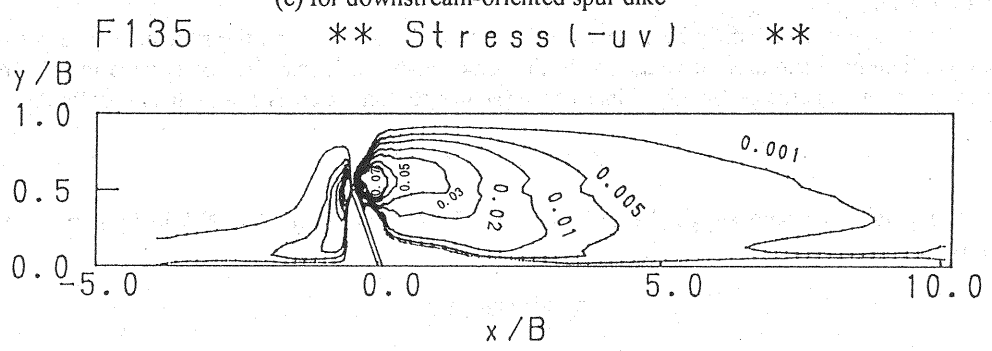

(d) for upstream-oriented spur dike

Fig. 9 Isobaric lines of the Reynolds stress -uv for the flow around the various spur dikes

downstream side of the spur dike which is defined as the longitudinal component of the distance from the downstream corner of the spur dike to the reattachable point, there is no apparent difference due to the variation of the spur dike configuration. But L-head spur dike can lower the eddy disturbance, and the center of the strength of eddy zone moves downstream slightly as compared with the normal spur dike (see Fig. 7 (a), Fig. 7 (b)). It is also found from Fig. 7 that with a decrease of the spur dike length, the recirculation length of the downstream sides of the spur dikes will be swiftly short, but it is not proportional to the spur dike length. Besides, Fig. 8 presents the calculated turbulent kinetic energy profiles of L-head spur dike and downstream-oriented spur dike. The values of the turbulent kinetic energy in the vicinity of the spur dike tip increase apparently. It indicates clearly that the mixing effect of the flow strengthen distinctly when the flow goes round the spur dike tip. Fig. 9 shows the calculated isolines of the Reynolds stress -uv of the various spur dikes (the scale is the same as that in Fig. 7). It is found that stronger eddy disturbance lies on the interface between main stream current and recirculating current and at the vicinity of the spur dike's tip. From Fig. 8 and Fig. 9, we can also find, the turbulent kinetic energy and Reynolds stress -uv vary in the same sense.

CONCLUSIONS

The depth-averaged k-ε model for the flow around the spur dikes can reproduce the experimental results satisfactory. And it has also provided the detail of the flow around the spur dikes. The improvement for conventional grid system is successful, thus, it provides engineers and numerical analysts with an alternative method to the boundary-fitted transformation which may not be easily obtained in many cases.

From above-mentioned results, the spur dike orientation angle will give larger influence to the stream current than its configuration, and the effective length is a more significant factor than its orientation angle. It is pointed out that, although the shorter spur dike length provides less proof to the bank, owing to the width of the river in alluvial plane being generally larger, and water depth being relatively shallow, the spur dike whose length is shorter compared with the river width is mostly used in actual engineering. And an array of spur dikes is being adopted to overcome its shortage. In addition, in the nearby corner of the spur dike, the calculated depth and velocities have certain error for comparison with the experimented values, it is because of there being the stronger secondary flow in the corner, the two dimensional model can only simulate the flow similarly. In order to simulate hydraulic characteristic of the flow around the spur dikes at the best, it is necessary to study three dimensional model.

Because many advanced calculational methods (such as BCT) are used in the present paper, computing time has been reduced significantly. For calculated grid with 30×100 for the downstream-oriented spur dike, it takes about 10 minutes to reach convergence (residual norm less than 0.001) on PC-9801BA computer.

The code has successfully been developed to solve the flow around the spur dikes which have certain configuration and arbitrary angles with the bank, moreover, it may be popularized to solve the problem of river constriction by other kinds of hydraulic structure (such as closing banks, cofferdams).

ACKNOWLEDGEMENT

We gratefully acknowledge the assistance of Mr. M.Ohashi and Mr. N.Mio in some of the measurements.

REFERENCES

1. Chieng, C.C. and B.E. Launder : On the calculation of turbulent heat transport downstream from an abrupt pipe expansion, Numerical Heat Transfer, Vol.3, pp189-207, 1980.
2. Iwasa, Y., T. Hosoda, J. Hiraoka, K. Okagawa : Resistance law of flows in headrace tunnel

without concrete lining, the Annuals of the Disaster Prevention Reserch Institute, Kyoto University, No.34, B-2, April, 1991 (in Japanese).
3. Latimer, B.R. and A. Pollard : Comparison of pressure-velocity coupling solution algorithm, Numerical Heat Transfer, Vol.8, pp.635-652, 1985.
4. McGuirk, J.J. and W. Rodi : Depth-averaged mathematical model for near field of side discharge into open- channel flow, Journal of Fluid Mechanics, Vol.86, pp.761-781, 1978.
5. Patankar, S.V. and D.B. Spalding : A calculation procedure for heat, mass, and momentum transfer in three-dimensional parabolic flows, Int. J. Heat Mass Transfer, Vol.15, pp.1787-1806, 1972.
6. Patankar, S.V. : Numerical Heat Transfer and Fluid Flow, Hemersphere, 1980.
7. Rodi, W. : Turbulence Methods for Environmental Problems, Hemersphere, 1979.
8. Tao, W. : Numerical Heat Transfer, Publishing House of Xi'an University of Communications, 1988 (in Chinese).
9. Tomonaga, A., J. Liu, N. Mio, and M. Ohashi : Experimental study on the effects of spur dike orientation angle, 49th Annual Conference of JSCE,2-A, pp.302-303,1994 (in Japanese).
10. Tsakiris, G.P., J.V. Soulis and C.V. Bellos : Two-dimensional unsaturated flow in irregular shaped regions using a finite volume method, Transport in Porous Media, Vol.6, pp.1-12, 1991.
11. Van Doormaal, J.P. and G.D. Raithby : Enhancement of the SIMPLE method for predicting incompressible fluid flows, Numerical Heat Transfer, Vol.7, pp.147-163, 1984.

APPENDIX - NOTATION

The following symbols are used in this paper:

B	= width of inlet section;
C_f	= friction coefficient;
C_l	= empirical coefficient ($=C_\mu^{3/4}/k$);
C_μ, $C_{\varepsilon 1}$, $C_{\varepsilon 2}$, C_k, C_ε	= coefficients in turbulence model;
e^*	= dimensionless diffusivity;
F	= dimensionless coefficient;
g	= gravitational acceleration;
h	= local water depth;
k	= turbulence kinetic energy;
k_0	= inlet distribution of turbulence kinetic energy;
n	= Manning roughness coefficient;
P_h	= production of turbulence kinetic energy due to interaction of turbulent stresses with horizontal mean velocity gradient;
P_{kv},$P_{\varepsilon v}$	= source terms originating from non-uniformity of vertical profiles;
Re	= inlet Reynolds number;
S_ϕ	= source terms in equation (1);
u	= velocity component in x direction;
u_*	= shear velocity;
Uin	= velocity component of inlet section in x direction;
Um	= mean bulk velocity;
v	= velocity component in y direction;
V	= resultant velocity located at the center of the triangular control volume;

V_b = the componentof the resultant velocity V parallel to the face of the oriented spur dike

x = coordinate parallel to flow;

Δx = streamwise dimension of control volume (Fig.3);

y = coordinate normal to flow;

Δy = cross-stream dimension of control volume(Fig.3);

y_p = distance normal to solid wall;

z_b = bottom elevation;

Γ_u = diffusion coefficient representing momentum equation in x direction;

Γ_ϕ = generalized diffusion coefficients;

ε = dissipation rate of turbulence kinetic energy;

ε_0 = inlet distribution of dissipation rate of turbulence kinetic energy;

κ = von Karman constant;

ν = kinematic viscosity;

ν_{eff} = effective viscosity;

ν_t = turbulence kinematic viscosity;

ρ = mass density of fluid

σ_k, σ_ε, σ_t = turbulent Plandtl numbers;

τ_{bx}, τ_{by} = bed shear stress components in x and y coordinates, respectively; and

ϕ = dependent variable.